Chemical Geology 555 (2020) 119830

Contents lists available at ScienceDirect

Chemical Geology

journal homepage: www.elsevier.com/locate/chemgeo

U-Th zircon dating reveals a correlation between eruptive styles and repose periods at the Nisyros-Yali volcanic area, Greece

Răzvan-Gabriel Popa[a,*], Marcel Guillong[a], Olivier Bachmann[a], Dawid Szymanowski[a,b], Ben Ellis[a]

[a] Institute of Geochemistry and Petrology, ETH Zürich, Clausiusstrasse 25, 8092 Zürich, Switzerland
[b] Department of Geosciences, Princeton University, Princeton, NJ 08544, USA

ARTICLE INFO

Editor: Balz Kamber

Keywords:
Effusive-explosive transitions
U-Th disequilibrium dating
Zircon dating
Time dependency
Volcanic repose periods
Water supersaturated rhyolitic magma
Forecasting eruptive style

ABSTRACT

Water-rich silicic magmas are capable of erupting effusively and explosively, and this drastic change in eruptive styles, termed effusive-explosive transition, has important implications in managing volcanic hazards. Some volcanoes exhibit effusive-explosive transitions during the same eruptive event, while others show this behavior between different eruptions. In the latter case, magma chamber processes induce physical-chemical changes in the magma, which can favor either effusivity or explosivity. This is the case for the Nisyros-Yali volcanic center, from the South Aegean Sea. In the recent stages of activity (past 120 ky), the volcanic area generated eight rhyolitic effusive and explosive events (five on the island of Nisyros and three on the island of Yali), including two caldera-forming eruptions. Changes of water content, temperature and pre-eruptive water-saturation between effusive and explosive deposits point to a potential time-dependency between the two eruptive styles. We investigate this time-dependency by applying U−Th disequilibrium dating to zircon crystals. Our eruptive age estimates of the investigated units range from 118.7 ± 10 ka to 19.9 ± 1.5 ka for Nisyros, and from 40 ± 5.2 ka to 22.7 ± 1.6 ka for Yali. Yali volcano has developed after the two caldera-forming events on Nisyros, which occurred at 63.1 ± 4.7 ka and 58.4 ± 2.7 ka. Yali marks the transition to a more geometrically complex system, where the upper-crustal silicic mush hosts at least two eruptible magma chambers (one under Yali, and one under Nisyros). The eruptive styles at both volcanoes seem to be correlated with the length of the repose periods. Effusive events occur after longer periods of volcanic quiescence, while explosive events are generated after shorter periods of repose of ~5–10 ky, which can be extended based on eruption age uncertainty to < 18 ky for Nisyros and < 12 ky for Yali. This observation is explained by the physical state of the volatiles in the magma chamber, with longer repose periods favoring volatile build-up. This can lead to water-supersaturation at storage pressures which was shown to favor effusivity. Based on this interpretation, both Nisyros and Yali volcanoes are presently in the effusive time window, which makes it probable for the next eruptions to be non-explosive.

1. Introduction

Effusive-explosive transitions are volcanic phenomena that induce the shift from one style of eruption, to another. They occur regularly at most subaerial volcanoes and can pose numerous hazards, especially when the transition involves a change from an effusive eruption, to an explosive event. When these shifts take place during the same eruptive event, they are closely coupled to conduit processes (Cassidy et al., 2018), which occur on relatively short timescales during syneruptive magma ascent. As a result, effusive-explosive transitions are difficult to predict if they transpire as an eruption is ongoing. Even if predicted, the short timescales characteristic of conduit processes leave little that can be done in terms of mitigation. However, in many cases effusive-explosive transitions occur between independent, distinct eruptions. There are many examples of active volcanoes where effusive and explosive events of compositionally similar silicic magmas are separated by a repose time, ranging from years to millennia. These include Nisyros-Yali in the South Aegean Arc (Di Paola, 1974), Quizapu in Chile (Ruprecht and Bachmann, 2010), or Ciomadul in Romania (Laumonier et al., 2019). Given the time gap between different eruptive events of contrasting style, this type of effusive-explosive transition is potentially closely related to magma chamber processes. These longer-term processes significantly change the thermo-chemical properties of the magmas and can modify the feedbacks that occur later, during conduit ascent (Ruprecht and Bachmann, 2010; Cassidy et al., 2016; Degruyter et al., 2017; Popa et al., 2019, 2020). The timescales required for

* Corresponding author.
E-mail address: razvan.popa@erdw.ethz.ch (R.-G. Popa).

https://doi.org/10.1016/j.chemgeo.2020.119830
Received 15 July 2020; Received in revised form 11 August 2020; Accepted 14 August 2020
Available online 18 August 2020

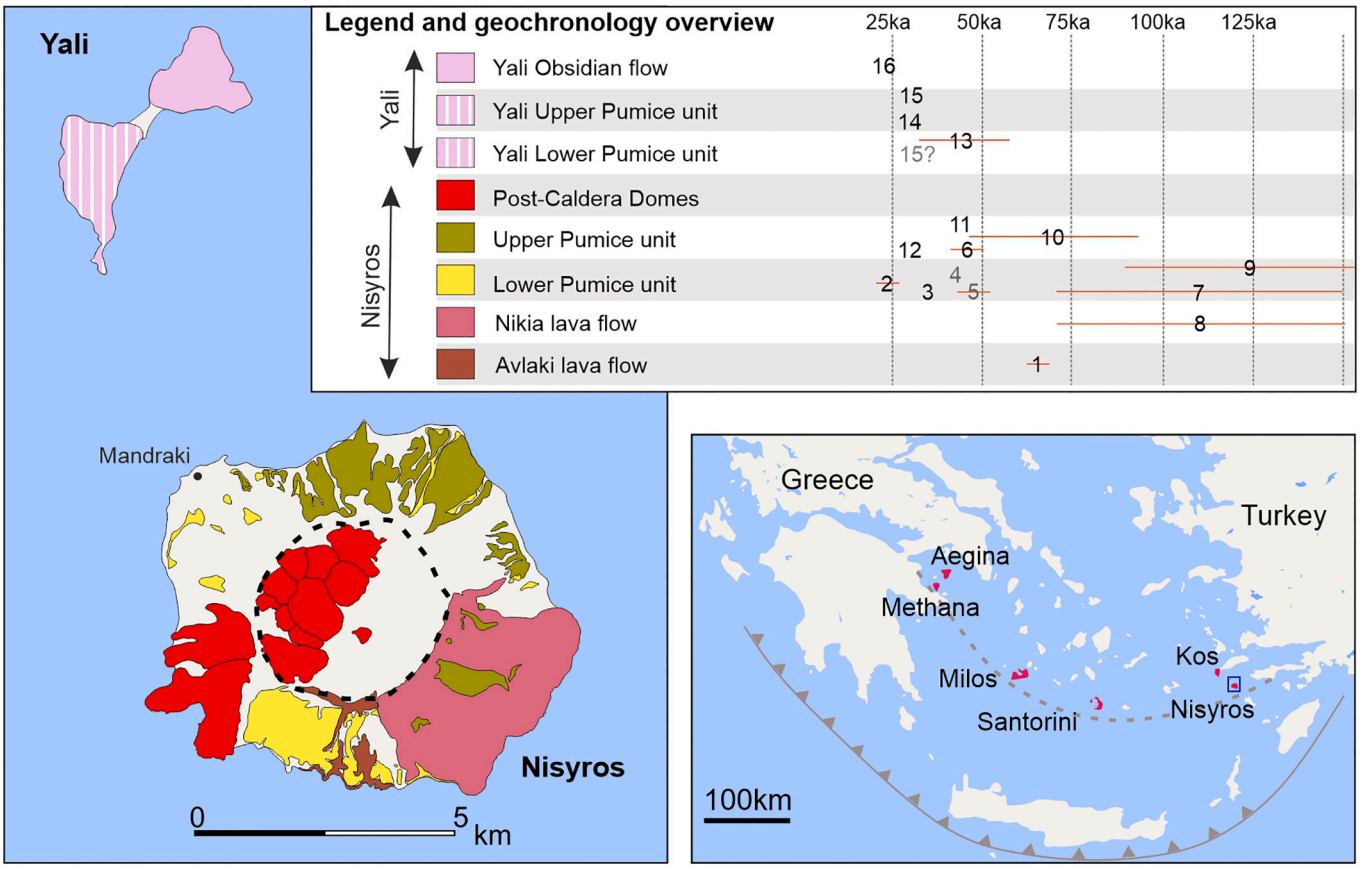

Fig. 1. Simplified geological map of Nisyros and Yali volcanoes (after Dietrich, 2018) indicating the 8 rhyolitic/rhyodacitic events that are dated in this paper. The regional inset shows the location of the subduction front and volcanic arc (after Pe-Piper and Piper, 2005). Next to the legend, we provide age estimates available in the literature. The geochronology compilation is from: (1) Rehren (1988) 66.6 ± 2 ka K-Ar, (2) Rehren (1988) 24 ± 0.56 ka ^{14}C, (3) Hardiman (1999) 35 ka extrapolation based on linear sedimentation rate in marine drill cores, (4) Aksu et al. (2008) 42–44 ka extrapolation using oxygen isotope stratigraphy in marine drill cores, (5–6) Margari et al. (2007) and Pyle and Margari (2009) 46.8 ± 5.7 ka, 46 ± 5.7 ka AMS radiocarbon dating in marine drill cores, (7) Barberi et al. (1988) 110 ± 40 ka fission track in volcanic glass, (8–10) Guillong et al. (2014) 111 ± 42 ka, 124 ± 35 ka, 70 ± 24 ka LA-ICP-MS U—Pb zircon dating maximum ages, (11) Limburg and Varekamp (1991) > 44 ka ^{14}C dating in charcoal, (12) Vinci (1985) 31 ka calculated by extrapolation of sedimentation rates in drill cores, (13) Guillong et al. (2016) 45 ± 10 ka U-Th maximum age, (14) Federman and Carey (1980) 31 ka correlated from oxygen isotope stratigraphy, (15) Satow et al. (2015) 33 ± 0.5 ka, (16) Wagner et al. (1976) 24 ka fission track on volcanic glass. It is unclear whether the age estimated by Satow et al. (2015) is related to the Lower or Upper Yali event. We note that ages (4) and (5) provided for the Lower Pumice tephra of Nisyros seem to have been estimated on potentially reworked Upper Pumice tephra (Tomlinson et al., 2012) and might not represent actual eruptive ages for neither of the two units.

magma chamber processes to take place are usually quantifiable (Szymanowski et al., 2017, 2019), potentially making this specific type of effusive-explosive transition possible to forecast.

Nisyros and Yali volcanoes in Greece are relevant case studies. These volcanoes have generated a series of independent rhyolitic effusive and explosive eruptions, and still have active magma chambers (Fig. 1, A). They are part of the Kos-Nisyros magmatic system, responsible for the largest Quaternary eruptions of the South Aegean Arc (Bachmann et al., 2019). The timeline of the volcanic activity at Nisyros and Yali is poorly constrained, with only a few, generally inconsistent ages available (overview in Fig. 1, B). The volcanic activity of Nisyros started after the 161 ka caldera collapse of Kos (Bachmann et al., 2012). Nisyros developed at the rim of the Kos caldera as an underwater basaltic andesite structure that later progressed to a stratovolcanic island (Di Paola, 1974). In the more recent stages of activity, post 120 ka (Fig. 1, B), the volcano persistently generated effusive and explosive rhyolitic eruptions (Dietrich, 2018). The system produced two Subplinian caldera-forming events, marked by the emplacement of the Lower and Upper Pumice deposits. It also generated three rhyolitic effusive eruptions, which have occurred before and after the explosive events: the Avlaki and Nikia lava flows, and the Post-Caldera Domes. The growth of the island of Yali began after the caldera collapse of Nisyros, producing two rhyolitic explosive events which emplaced the Lower and Upper Yali Pumices, and a voluminous obsidian lava flow (Bachmann et al., 2019).

Our previous work focused on these eruptive units and showed that the repeated change in eruptive style at Nisyros-Yali is influenced by magma chamber processes (Popa et al., 2019). According to this previous work, all rhyolitic and rhyodacitic eruptions were triggered by the interaction between hot recharge material and upper-crustal rhyolitic magmas. At the time when explosive events took place, the upper-crustal magmas were water-rich (~4.5 wt% H_2O), but water-undersaturated. In contrast, effusive events were generated from upper-crustal magmas that were, paradoxically, richer in water (~5.5 wt% H_2O), but water-supersaturated at magmatic storage conditions. In short, when comparing explosive and effusive deposits at Nisyros-Yali, there is one major consistent difference that occurs in the magma chamber. Namely, this is the absence (explosive) versus presence (effusive) of exsolved volatiles during pre-eruptive magmatic storage (Popa et al., 2019).

The mechanical influence of pre-eruptive exsolved volatiles on triggering effusive-explosive transitions is thoroughly discussed in Degruyter et al. (2017) and Popa et al. (2019). Briefly, the presence of exsolved volatiles in the magmatic reservoir increases its bulk

compressibility. In the event of a magmatic recharge, the compressibility of the gas 'bubbles' acts to delay eruption triggering, by reducing the volume occupied by the exsolved gas to accommodate the incoming recharge material. Effectively, this means that higher volumes of recharge are required to induce the critical overpressure needed to trigger the eruption. Higher volumes of recharge magma and delayed eruption triggering lead to a more intense reheating of the subvolcanic magma reservoir, which lowers the viscosity of the melt. The lower viscosity concurs with the pre-eruptive presence of exsolved gas to induce early gas permeability and enhanced outgassing in the conduit. Hence, this situation diminishes the explosive potential of the ascending magma, increasing the probability of an effusive event.

We have previously suggested two endmember scenarios for the rhyolitic effusive-explosive transitions at Nisyros and Yali, which can combine to various extents: the space-dependent and the time-dependent models (Popa et al., 2019). In a space-dependent situation, the upper-crustal mush contains multiple eruptible melt pockets that are stored under different conditions. Hence, water-supersaturated and water-undersaturated eruptible melts could coexist as separate magma bodies. In this case, the eruption style is a function of which melt pocket is tapped by the eruption-triggering recharge. In a time-dependent model, each volcano has a primary magma chamber that can, in time, change between water-undersaturated and water-supersaturated states. These changes can be caused, for example, by syneruptive outgassing (water loss) or by differentiation (water gain). In a time-dependent model, an eruption of a water-rich magma would leave behind a water-poorer, undersaturated magma chamber that is rejuvenated by mafic recharge. After rejuvenation, this magma chamber resumes its differentiation path, with a progressive increase in volatiles with time. Explosive eruptions are favored during the water-undersaturated stages of differentiation. Given enough repose time, the magma chamber could reach water-supersaturation once more. At this point, effusive eruptions are favored. Here, we aim to test whether a space-dependent or a time-dependent model dominates the effusive-explosive transitions at Nisyros-Yali. If a time-dependent control is dominant, there should be a distinct difference in the repose periods preceding effusive and explosive events.

The Nisyros-Yali units are particularly complicated to date. They are mostly too old for C^{14} (or have very little charcoal preserved), and are characterized by the absence of major K-bearing phases and/or ^{40}Ar excess (Bachmann et al., 2010). Hence, some combination of U-Th-Pb dating, preferably of zircon, is the optimal solution for this system. U—Pb zircon ages are available for some of the units (Fig. 1, B), but given the young activity of the volcanoes (low Pb concentration), the results are not particularly reliable (Guillong et al., 2014; Guillong et al., 2016). Here, we use zircon crystals for U—Th disequilibrium dating, a method suitable for volcanic rocks younger than ~300 ky (Lowenstern et al., 2000; Schmitt, 2011). We determine the crystallization ages of individual zircons, and we use the youngest ages to approximate the timing of the eruptions. This is an excellent first assessment of eruptive ages, which can be further refined by implementing (U—Th)/He dating (Danišík et al., 2016).

2. Materials and methods

Fresh rock samples were collected from the eight units mentioned above (Fig. 1). In the case of the post-caldera event, we analyzed samples from the Trapezina dome. The crystals were separated from the matrix using high voltage fragmentation (SELFRAG). Due to the zircon-poor nature of the samples, aliquots of crushed material were treated with dilute HF, which resulted in dissolution of matrix glass and most mineral species. Zircon crystals generally < 50 μm in size were hand-picked from the residue under a stereographic microscope. The crystals were mounted in epoxy-resin and exposed by grinding with aluminum-oxide paper, followed by polishing using diamond suspension. The epoxy mounts were carbon coated and the zircon crystals were verified for the presence of inherited cores using cathodoluminescence (inherited cores were not observed).

Laser Ablation Inductively Coupled Plasma-Mass Spectrometry (LA-ICP-MS) was used to determine the $^{230}Th/^{232}Th$, $^{238}U/^{232}Th$ and $^{238}U/^{230}Th$ ratios of individual zircon crystals. We used a Resonetics Resolution S155 laser ablation system connected to a Thermo Element XR sector-field mass spectrometer at ETH Zürich. The laser spots were set to a diameter of 29 μm. The laser was configured to a repetition rate of 5 Hz and a fluence of 2.5 Jcm^{-2}. The duration of the ablation was 30 s on the gas blank and 40 s on the sample. Given the small size of the zircon crystals, most of them could only accommodate one ablation spot per grain.

The gas blank corrected intensities, including uncertainties on the ratios, were derived using the SILLS software (Guillong et al., 2008). Complete data reduction that yields the U—Th isotope and activity ratios was performed using a spreadsheet following the methodology described in Guillong et al. (2016). The procedure consists of correcting for: (1) interferences on ^{230}Th caused by polyatomic zirconium oxides generated during ablation, (2) the abundance sensitivity effect of ^{232}Th on ^{230}Th, which is estimated using monazite measurements, and (3) the relative sensitivity factor using zircon 91500 as reference material. The accuracy of the measurements and correction routine was verified against validation reference materials that are in U—Th secular equilibrium. The reference materials were repeatedly measured throughout the analytical sessions and treated as unknowns during data processing. These included the 91500 (Wiedenbeck et al., 1995), Temora (Black et al., 2004), Plešovice (Sláma et al., 2008) and Fish Canyon Tuff (Schmitz and Bowring, 2001) zircons.

The isotopic ratios of the groundmass glasses were analyzed by LA-ICP-MS. We used a similar setup to the one described above, with laser spots of 163 μm, repetition rate of 10 Hz and fluence of 3.5 Jcm^{-2}. The data reduction procedure was similar to that applied to zircons, but without the polyatomic oxide correction which was unnecessary in this case. NIST612 (Hollocher and Ruiz, 2007) and BCR-2G (Rocholl, 2007) were run as secondary standards.

The isotopic ratios of the bulk-rock samples were analyzed with a ThermoScientific NeptunePlus Multicollector Inductively Coupled Plasma-Mass Spectrometer (MC-ICPMS) at the New Mexico State University. The samples were powdered and dissolved in HF, HNO_3 and HCl, they were split and equilibrated with ^{236}U and ^{229}Th spikes on a hot plate for three days. The samples were purified using anion exchange resin, 7 N HNO_3 and 6 N HCl acids. The isotopic ratios were measured in static mode using Faraday collectors or electron multipliers. $^{230}Th/^{232}Th$ ratios were normalized to ThA (171500) and U ratios were normalized to U-010 to correct for mass bias and yield. The complete procedure is available in Ramos et al. (2016).

The sampling locations, U—Th ratios of zircon crystals, and isotopic compositions of groundmass and bulk-rocks can be found in the electronic supplementary files.

3. Data discussion

All analyzed zircon crystals display $^{230}Th—^{238}U$ disequilibrium with variable degrees of U-excess, which allows us to calculate model ages for all investigated units (Fig. 2). Data from individual eruptions do not describe clear isochrons, but rather plot as sphenochrons, also known as "time wedges" (Chen et al., 1996). Sphenochrons suggest prolonged crystallization over several time periods that were favorable for zircon growth, leading to the accumulation of multiple zircon age populations (Schmitt, 2011). This type of protracted crystallization might lead to an overestimate of the eruption age, as many zircon crystals (or zircon parts) have grown at considerable times before the eruption. A Gaussian approach to calculating the ages (Lowenstern et al., 2000) would fail to indicate a time period close to that of the eruption, but would likely reflect the time period when magmatic conditions were most favorable for zircon growth, which might not necessarily coincide with the

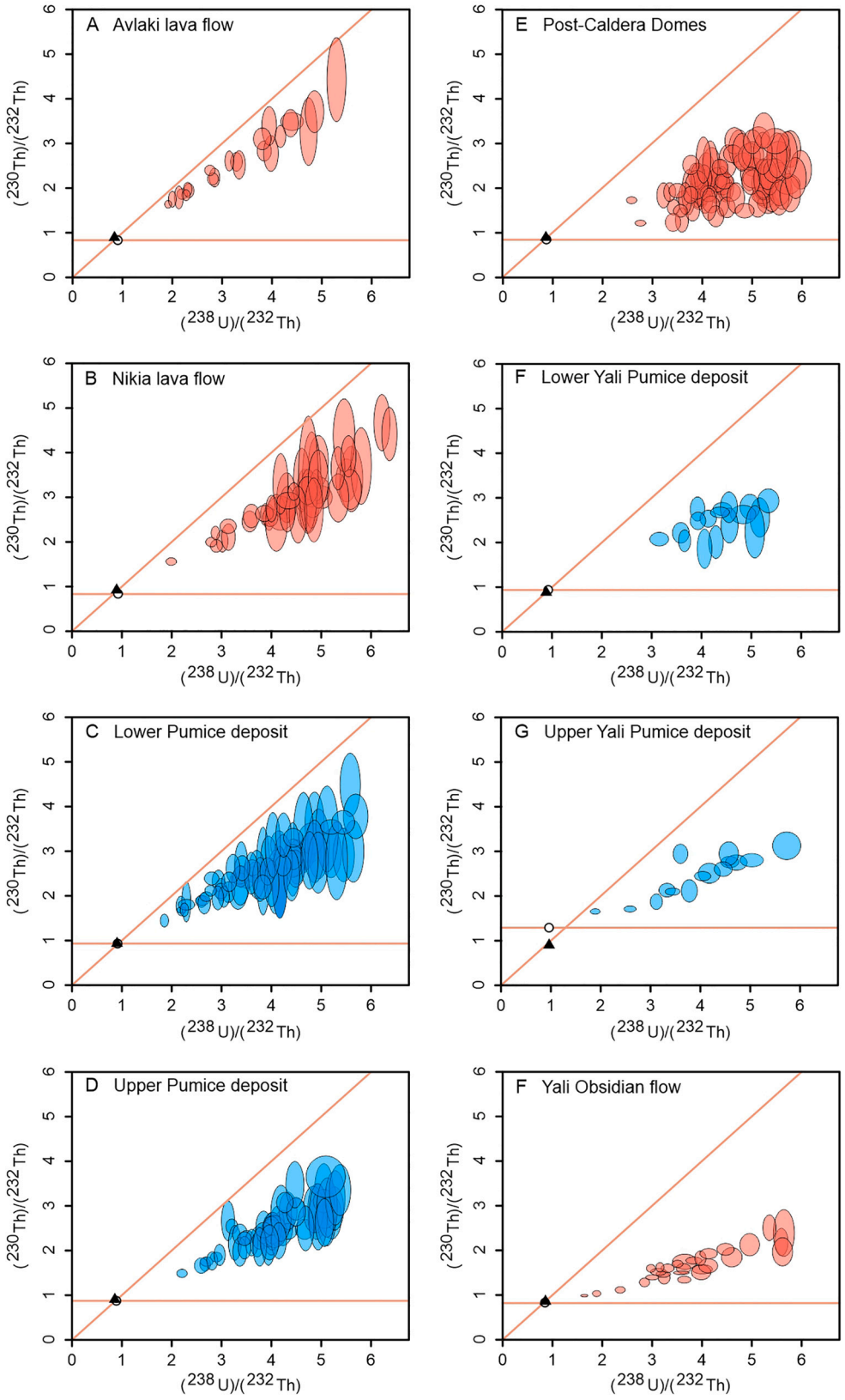

Fig. 2. Activity ratio diagrams for $^{238}U/^{232}Th$ and $^{230}Th/^{232}Th$. Red indicates effusive, and blue explosive deposits, uncertainty is 1 sigma. The orange lines indicate the equiline (diagonal) and present-day line (horizontal). The open circles and the black triangles mark the isotopic activity ratios of the groundmass glasses and of the bulk-rocks, respectively. (For interpretation of the references to color in this figure legend, the reader is referred to the web version of this article.)

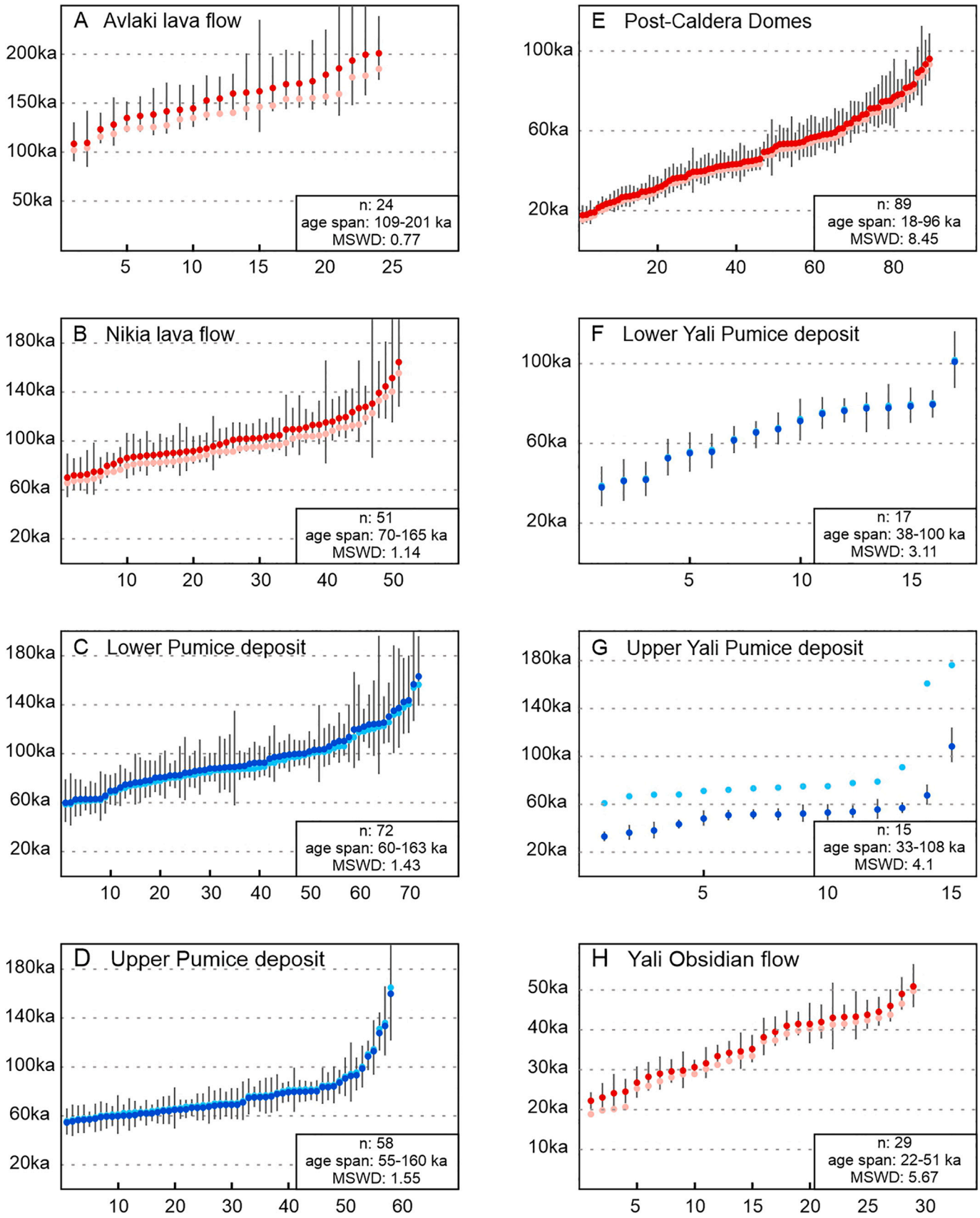

Fig. 3. Overview of crystallization timescales for each unit, based on calculated model ages. Red stands for effusive and blue for explosive events, respectively. Deep colors indicate model ages calculated using the isotopic composition of the groundmass glasses (1σ error bars plotted). Light colors indicate the use of bulk-rock isotopic compositions (error bars are of similar extent, not plotted). The text boxes indicate the number of crystals analyzed (n), the total age span recorded and the global MSWD of each dataset. (For interpretation of the references to color in this figure legend, the reader is referred to the web version of this article.)

youngest stages of zircon crystallization.

To estimate the ages of individual crystals, we calculate two-point zircon-melt isochrons, similarly to Harangi et al. (2015). We can calculate two different sets of ages, relying on (1) the groundmass glass and (2) the bulk-rock isotopic ratios, which we use as estimates of the initial isotopic composition of the melt at the time of zircon crystallization. The 'initial' melts have $^{230}Th/^{238}U$ activity ratios close to secular equilibrium (median of 0.99 for the groundmass glass and 1.01 for the bulk-rock), which allows us to generate two-point model ages - it is expected that the initial isotopic melt composition is close to equilibrium, since the crystallization of zircon is likely to be the main cause of isotopic fractionation (e.g. Harangi et al., 2015).

Using initial isotopic estimates obtained from groundmass glass or bulk-rock compositions yields similar results, which are generally within error of each other (Fig. 3). The age differences between the two datasets tend to become insignificant for the younger zircon crystals, generating differences of 2 to 6 ky. In essence, any of the two isotopic compositions can be used to calculate relevant zircon model ages. However, since we are more interested in precisely determining the crystallization age of the **youngest** zircons, which should be closer to the actual eruption age, we prefer using the groundmass glass isotopic composition as an intercept for the two-point isochrons. The matrix glass is expected to be isotopically similar to the melt that crystallized the youngest minerals and hence, it is reasonable for the ages of the youngest zircon crystals to be more accurate if we use the groundmass glass isotopic conditions. This is a valid assumption for Nisyros-Yali, since no significant melt hybridization occurred prior to eruption triggering, despite recharge and magma mingling taking place (Popa et al., 2019). Therefore, in the following discussion we will refer only to the model ages derived using the isotopic composition of the matrix glasses.

Interestingly, in the case of the Upper Yali unit we are unable to calculate a geologically relevant eruption age by using the bulk-rock isotopic activity ratios: the age appears older than the Lower Yali even outside uncertainty, although the Upper Yali clearly overlies this unit stratigraphically. We are able to obtain an age in agreement with stratigraphy by using an average of the isotopic activity ratio of the groundmass glass only (the glass does show some variations in $^{230}Th/^{232}Th$, despite the rock samples being fresh). A possibility regarding this particular unit, considering the low zircon yield, small zircon size and higher storage temperature compared to the other units (~850 °C, Popa et al., 2019) is for the zircon to be partly resorbed. In this case, if we are to consider the bulk-rock isotopic activity ratios accurate (which are close to secular equilibrium), then the crystals do not record the latest stages of crystallization and this method might be unusable to date this particular eruption. Hence, we recommend that the age we report for the Upper Yali tephra to be considered as approximate, and it can be amended in the future. Despite this caveat, we are still able to crosscheck our Upper Yali eruption age estimate with others from the literature (see Section 4.2).

The challenge at this point is in determining eruptive ages that are reasonably accurate based on the model crystallization ages calculated for each unit (Fig. 4). We approach this issue in three different ways: (1) the youngest zircon method (e.g. Wotzlaw et al., 2013), (2) Bayesian modelling (Keller et al., 2018) and (3) the youngest zircon population method (results in Table 1). We calculate Bayesian eruption age estimates assuming uniform and triangular zircon age distributions, and a zircon crystallization distribution based on kinetic and (MELTS) thermodynamic models (Keller et al., 2018). The results are insensitive to the assumed distribution, and are available in the Supplementary files and illustrated in Fig. 4B. The youngest zircon population method relies on an Iterative-MSWD approach, with the iteration starting from the youngest pair of zircon crystals (n = 2). We gradually add progressively older crystals to the test pool (n++) and calculate the MSWD each time. Because larger single-age uncertainties might hide relevant geological processes, such as protracted crystallization, we choose the youngest population based on the visual interpretation of the change in this parameter, as crystals are being added to the test pool. In the example provided in Fig. 4A, the first six youngest crystals form a coherent age population, before the rate of change of the Iterative-MSWD increases at n = 7. We determine the age of the youngest zircon population by calculating the weighted mean of the individual ages, as a function of the uncertainties. The uncertainty of the weighted mean age is 1σ, generated using the equations from IsoplotR (Vermeesch, 2018). For Nisyros-Yali, the youngest population ages are estimated based on groups of 3 to 13 crystals.

The three different methods provide similar eruptive age estimates for the five youngest eruptions at Nisyros-Yali, but diverge for the three oldest units (Table 1, Fig. 4B). The ages are generally within error of each other, specifically the *youngest zircon* and *youngest zircon population* ages. All three methods have specific advantages and caveats, that we discuss in the following.

The youngest zircon method, albeit being less precise, could provide a more accurate eruption age estimate. This is simply because relying on a single crystal eliminates the effect of protracted crystallization, which could lead to overestimating eruption ages. This is always a risk when applying U—Th or U—Pb crystal dating, because zircon tends to record long crystallization histories, as discussed further below. However, when relying on a single crystal there is the equivalent risk of underestimating the age. By using a single data point it is not possible to eliminate the effect of a statistical Gaussian distribution, which could lead to the youngest zircon age being actually younger than the eruption age. In our specific case, we observe that the single-crystal age has a relatively large uncertainty that might lead to imprecision, particularly in cases where this uncertainty is large in comparison to the apparent spread of all dates (e.g. Avlaki, Nikia lava flows). While the youngest zircon approach may be more robust in cases with a high global MSWD (e.g. Post-Caldera Domes), we do not favor it as being the most reliable for our dataset.

The Bayesian and the Iterative-MSWD methods yield eruption ages with comparable uncertainties. For the Upper Pumice, Post-Caldera Domes and the three Yali eruptions the difference between the ages given by the two methods is less than 2500 years, and within uncertainty. However, for the older Lower Pumice, Nikia and Avlaki eruptions the difference increases to > 10,000 years. For these specific units, the Bayesian method yields progressively older eruption ages than the Iterative-MSWD.

The divergence between the two methods is linked to the progressively larger uncertainties that are associated with the U—Th disequilibrium dating of progressively older units. The larger uncertainties result in a global MSWD close to or less than 1, which makes different age populations and prolonged crystallization less discernible from a statistical point of view. From a geological point of view, however, prolonged crystallization is still likely present. All the younger units (Post-Caldera Domes and the Yali eruptions) clearly show zircon crystallization over long periods of time, spanning 30 to 80 ky, with MSWDs as large as 8 (Fig. 3E–H), as suggested for many other systems (see for example, Simon et al., 2008). Similarly, albeit statistically obscured by larger uncertainties, the older units of Nisyros also record protracted crystallization of zircon. This is indicated by the maximum zircon ages of ~160 ka in the oldest units, coinciding with the age of the massive, pre-Nisyros Kos Plateau Tuff eruption (Bachmann et al., 2012), and decreasing over a time-span of nearly 100 ky. This is supported by the sphenochrons suggesting multiple zircon populations (Fig. 2).

Despite the few differences between the eruption ages derived with the Bayesian and Iterative-MSWD methods, the two sets of ages point to the same interpretation regarding the repose periods preceding each eruption style (discussed later in Section 4.4). However, stratigraphic constraints on the oldest of the investigated units, the Avlaki lava flow, indicates that the Bayesian method may slightly overestimate the eruption ages of the older units dated by U—Th. The Bayesian age estimate for the Avlaki lava flow is between 138.3 ± 7.3 ka and 135 ± 10.2 ka, while the recently dated, *stratigraphically older* Kyra

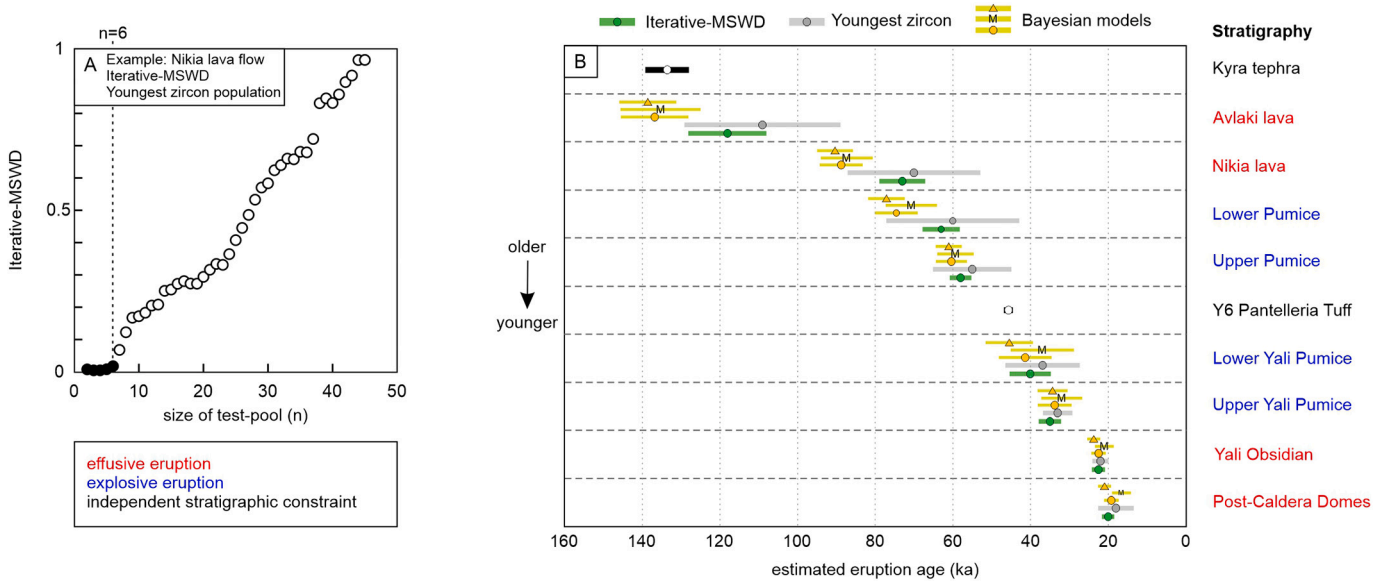

Fig. 4. Comparison of eruption ages estimated using the three different methods. A: Example of identifying the youngest zircon population by applying the Iterative-MSWD to the Nikia lava flow dataset. By successively pairing the youngest 6 zircon ages (n = 6) the MSWD changes at a low rate compared to n = 7, suggesting the same age population for the youngest 6 crystals. The value of the Iterative MSWD increases steeply as new zircons are added to the test-pool, indicating the addition of crystals from multiple age populations. B: Comparison of eruption ages (with 1σ uncertainty) estimated by the youngest population method (Iterative-MSWD), youngest zircon method, and Bayesian modelling assuming a uniform (circle), melts modelled (M) and triangular (triangle) prior distribution (Keller et al., 2018). The zircon-derived eruption age of the Kyra formation, which is an important stratigraphic constraint for the Avlaki lava flow, is referenced from Gençalioğlu-Kuşcu et al. (2020). The age of the Y6 Green Tuff of Pantelleria, a potential constraint for the Upper Pumice of Nisyros, is referenced from Scaillet et al. (2013). (For interpretation of the references to color in this figure legend, the reader is referred to the web version of this article.)

formation (andesitic tephra) has a zircon age of 133.5 ± 5.4 ka (Gençalioğlu-Kuşcu et al., 2020). Although the two age estimates are within uncertainty of each other, the highest probability age for Avlaki is older than the highest probability age of the Kyra formation. On the other hand, the Iterative-MSWD yields for Avlaki a young-population age of 118 ± 10 ka, outside 1σ uncertainty of the Kyra formation. Although the Bayesian approach may appear statistically stronger, this observation indicates that the Iterative-MSWD age of Avlaki may be the more geologically reasonable.

For our specific case, we observe that the Bayesian, Iterative-MSWD (youngest zircon population) and youngest zircon crystal approaches give comparable results for units younger than ~60 ky, but the Bayesian might overestimate the ages of the older units. Henceforth, for consistency we will rely throughout this paper on the eruptive ages estimated with the Iterative-MSWD, representing the crystallization age of the youngest zircon population. We consider the Iterative-MSWD to be a good trade-off between the youngest single crystal (which might underestimate the age, and is less precise) and the Bayesian method (which might overestimate it). We stress that irrespective of the method used, the main conclusions of the paper remain the same. Having discussed their advantages and caveats, we report the ages and repose periods calculated with each of the three methods in Table 1.

4. Implications

4.1. Volcano stratigraphy

The eruption ages that we obtain range from 118.7 ± 10 ka to 19.9 ± 1.5 ka for Nisyros, and from 40 ± 5.2 ka to 22.7 ± 1.6 ka for Yali. We are able to cross-check the age of the Yali Obsidian estimated by Wagner et al. (1976) and the age of the Upper Yali Pumice estimated by Federman and Carey (1980). We can also confirm the observation of Allen and McPhie (2000) that the Yali explosive events have occurred before the Post-Caldera Dome eruptions on Nisyros. We generally

Table 1
Eruption ages and repose periods determined by the youngest zircon, Bayesian uniform distribution model and youngest zircon population (Iterative-MSWD) methods. Uncertainty is reported as 1σ. The uncertainty of the repose periods is calculated using the quadrature method. The results of the Bayesian modelling using triangular and MELTS prior distributions are available in the Supplementary files and illustrated in Fig. 4B.

Volcano	Unit	Eruption age estimate (ka)			Preceding repose time estimate (ky)		
		Youngest zircon	Bayesian model	Youngest zircon population	Youngest zircon	Bayesian model	Youngest zircon population
Nisyros	Avlaki lava flow	108.7 ± 19.7	136.6 ± 8.7	118.7 ± 10	N/A	N/A	N/A
	Nikia lava flow	70.4 ± 17.6	88.7 ± 5.5	73.3 ± 5.8	38.3 ± 26.4	47.8 ± 10.3	45.4 ± 11.6
	Lower Pumice unit	59.9 ± 17.1	74.3 ± 5.5	63.1 ± 4.7	10.5 ± 24.5	14.4 ± 7.8	10.2 ± 7.5
	Upper Pumice unit	54.9 ± 10.5	60.4 ± 3.9	58.4 ± 2.7	5 ± 20	13.8 ± 6.7	4.7 ± 5.4
	Post-Caldera Domes	17.9 ± 4.6	19.2 ± 1.8	19.9 ± 1.5	37 ± 11.4	41.2 ± 4.3	38.5 ± 3.1
Yali	Lower Yali Pumice	37.8 ± 9.5	41.3 ± 6.8	40 ± 5.2	N/A	N/A	N/A
	Upper Yali Pumice	33.3 ± 3.7	33.8 ± 4.3	35 ± 2.8	4.5 ± 10.2	7.5 ± 8	5 ± 5.9
	Yali Obsidian flow	22.3 ± 2	22.5 ± 1.8	22.7 ± 1.6	11 ± 4.2	11.3 ± 4.7	12.3 ± 3.2

confirm the relative ages of the units (Dietrich, 2018), but we bring one correction to the relation between Nikia and the Lower Pumice event. The two units are found together on the SE coast of the island, but the exact relationship is ambiguous because the contact is not well exposed. Limburg and Varekamp (1991) have interpreted that Nikia overlies the Lower Pumice, and since then, in the absence of geochronology data the Lower Pumice was considered older (Dietrich, 2018). However, no heating, welding, alteration or deformation is observed in the pumice deposit along the contact with the lava flow. We argue that this is more likely a vertical contact, where the pyroclastic density currents generated by the Lower Pumice event were buttressed by the pre-existing Nikia lava flow. According to our geochronology data and to our field interpretation, the Nikia lava flow precedes the Lower Pumice event. This is in accordance with the initial interpretation of Di Paola (1974).

4.2. Deep sea tephrostratigraphy

Tephra layers from Nisyros, initially believed to have been generated during the Lower and Upper Pumice events, have been found in deep sea cores at various locations throughout the Aegean Sea (Vinci, 1985; Hardiman, 1999; Margari et al., 2007; Aksu et al., 2008; Pyle and Margari, 2009; Tomlinson et al., 2012). Indirect dating by linear extrapolation of sedimentation rates, by oxygen isotope stratigraphy and AMS radiocarbon ages (Fig. 1B), agree that these two tephra layers were sedimented in the Aegean roughly between 42 and 47 ± 6 ka (Aksu et al., 2008; Margari et al., 2007; Pyle and Margari, 2009). Later, they have both been reported as equivalent to the Upper Pumice eruption of Nisyros (Tomlinson et al., 2012).

However, the relative position of the Upper Pumice tephra in respect to the 45.7 ± 1 ka Y6 Green Tuff of Pantelleria (Scaillet et al., 2013) gives rise to an interesting conundrum. It has been reported to both overlie, and underlie it. For example, Margari et al. (2007) identify the ML-3 and ML-4 tephra overlying the Green Tuff, and both layers are attributed to the Upper Pumice event based on glass geochemistry (Tomlinson et al., 2012). The authors also identify the ML-6 tephra which is stratigraphically older than the Y6 marker, and is attributed to a potentially unidentified eruption from Nisyros. Also based on glass geochemistry, Karkanas et al. (2015) attribute another tephra layer to the Upper Pumice event of Nisyros, but this time underlying the Green Tuff of Pantelleria (in Theopetra Cave, mainland Greece). It is possible for the tephra identified by Karkanas et al. (2015) to be equivalent to the ML-6 tephra of Margari et al. (2007), both underlying the Y6 marker and having Nisyros-type rhyolitic compositions. However, there is one outstanding question. Which of the tephra deposits was really generated by the Upper Pumice eruption: the one younger, or the one older than the Y6 marker?

Overall, our zircon dataset supports the idea of the Upper Pumice of Nisyros being older than the Y6 Green Tuff of Pantelleria, with a *youngest zircon population age* of 58.4 ± 2.7 ka, a *Bayesian age* of 60.4 ± 3.9 ka (uniform prior) and a *youngest zircon age* (single crystal) of 54.9 ± 10.5 ka. At the same time, we do agree that our dataset does not fully resolve this conundrum. If the *youngest zircon age* is to be considered, the larger uncertainty associated to it could also support the possibility of the Upper Pumice of Nisyros being younger than the Y6 marker, and hence equivalent to ML-3 and ML-4 (Fig. 4B). The best solution to solve this is to refine our zircon ages with (U−Th)/He dating (Danišík et al., 2016).

We also point out that the glass major elemental composition of the Upper Pumice of Nisyros is very similar to that of the Yali Lower Pumice, the compositional fields partly overlapping (Popa et al., 2019). Hence, solely based on glass compositions it might not be possible to determine with certainty whether a tephra layer was generated by one event, or the other. To improve the accuracy of such a discrimination would require that all analyses, for both reference tephra and unknown tephra, be carried out in the same analytical session (to eliminate potential drifts, or differences induced by different calibration routines).

There is the possibility that the ML-3 and ML-4 tephra above the Y6, and the Theopetra tephra below the Y6, all belong to the Upper Pumice event of Nisyros. In this case, at least one of the stratigraphic records must have been affected by reworking. However, considering the similarity between the glass compositions of the Upper Pumice of Nisyros and the Yali Lower Pumice, there is another possibility that we would like to highlight, and leave open for future debate. Considering the relative position of these tephras in respect to the Green Tuff of Pantelleria (Y6), and our eruption age estimates:

- We suggest that the ML-6 and the Theopetra tephra underlying the Y6 could be correlated with the Upper Pumice event of Nisyros. Our preferred age is that of the *youngest zircon population*: 58.4 ± 2.7 ka. This is in agreement with Karkanas et al. (2015), who suggest an age older than 50 ka for the Upper Pumice, and it coincides accurately with the ML-6 age determined by Margari et al. (2007), of 58.5 ± 5.69 ka.
- We suggest that the ML-3 and ML-4 tephra overlying the Y6 marker could potentially be correlated with the Lower Yali eruption, which has a *youngest zircon population* age of 40 ± 5.2 ka, within error of 46 ± 5.69 ka as estimated by Margari et al. (2007).

In addition to placing the Upper Pumice event of Nisyros at 58.4 ± 2.7 ka, we estimate the age of the Lower Pumice event at 63.1 ± 4.7 ka. Also, the rhyolite cryptotephra dated at 33 ± 0.5 ka and 34.7 ± 2.5 ka by Satow et al. (2015) correlates with our age estimate for the Upper Yali explosive event (35 ± 2.8 ka).

4.3. Evolution of the Nisyros-Yali magmatic system

After the Kos Plateau Tuff event, the magmatic system of Nisyros required almost 40 ± 10 ky to evolve from basaltic andesite, to water-rich rhyolitic compositions. After the KPT event at ~160 ka, mafic magmas permeated the largely solidified and strongly reduced upper-crustal mush and generated the early underwater basaltic andesite eruptions at Nisyros (Bachmann et al., 2012). After it reached the surface, the seamount developed into a stratovolcano that erupted magmas of intermediate compositions, alternating between extrusions of dacites and andesites (Di Paola, 1974). The andesites likely reflect a part of the recharge magmas that still managed to erupt, while the dacites likely reflect the state of differentiation of the upper-crustal reservoir. In time, as the upper-crustal mush regrew and the magma chamber developed, it became more effective at trapping recharge material. As a result, the upper-crustal dacite eruptions became dominant and peaked with the extrusion of the voluminous Emborios domes (Dietrich, 2018; Popa et al., 2019). However, at 118.7 ± 10 ka the first rhyolites were extruded at Nisyros, generating the Avlaki lava flow.

At this point in time, after ~40 ± 10 ky of evolution, the Kos-Nisyros subvolcanic mush was primed for triggering major explosive eruptions (high volatile content, silica-rich, viscous melt). Nonetheless, the first two rhyolitic events that occurred at 118.7 ± 10 ka (Avlaki) and 73.3 ± 5.8 ka (Nikia) were both effusive. Explosive activity happened shortly after the Nikia lava flow, following a repose period of 10.2 ± 7.5 ky (Fig. 5A, B). At 63.1 ± 4.7 ka and 58.4 ± 2.7 ka the two major caldera-forming eruptions occurred on Nisyros: the Lower and the Upper Pumice events. Similarly to the larger KPT eruption, the two caldera collapse events of Nisyros led to a decompression of the upper-crustal reservoir that allowed the ascent of mafic magmas. Consequently, large volumes of basaltic andesite recharged the magma chamber of Nisyros after the Upper Pumice event (Popa et al., 2019). However, contrary to the KPT aftermath, the basaltic andesites did not erupt. This indicates that the upper-crustal mush retained the ability to effectively trap the recharge material. Approximately 38.5 ± 3.1 ky later, at around 19.9 ± 1.5 ka, voluminous water-rich rhyodacite domes were extruded both inside and outside the caldera. The extrusion of the Post-Caldera Domes indicates that the magma chamber of Nisyros

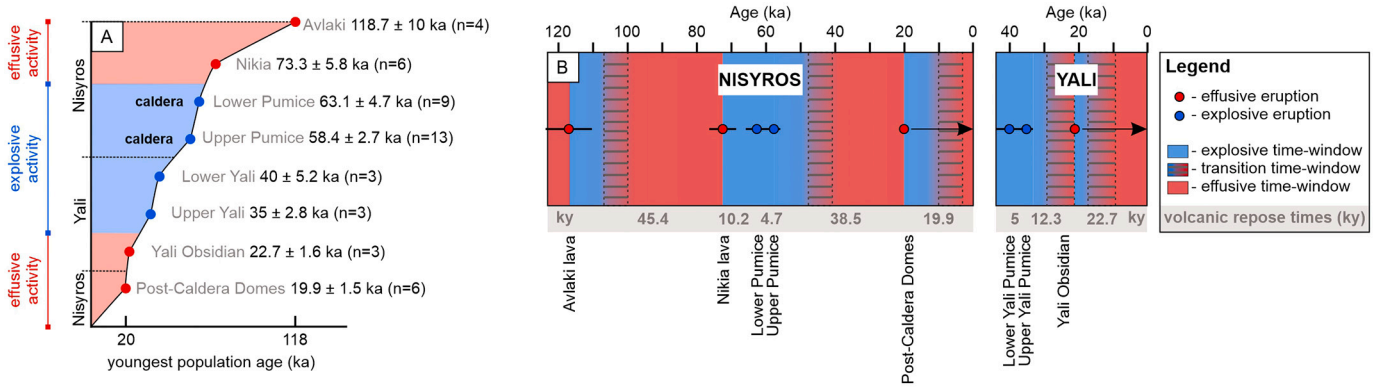

Fig. 5. Geochronological overview of the rhyolitic eruptive history of Nisyros and Yali volcanoes, highlighting the correlation between eruptive styles and volcanic repose periods. A: Overview of the eruption ages of the 8 investigated units (youngest population estimate, Iterative-MSWD), where red indicates effusive activity, and blue indicates explosive events. The numbers between brackets indicate the number of young crystals forming the age population. B: Overview of the relation between volcanic repose periods (time intervals given on the grey band) and eruptive styles at Nisyros-Yali. The blue fields mark explosive time windows, and the red fields mark effusive time windows. The hashed areas delimiting the transition from blue to red fields indicate the uncertainty associated to the explosive-effusive threshold (the error propagation of eruption age estimates calculated using the quadrature method). These could be interpreted as time periods where both eruptive styles are likely to occur. Uncertainty is 1σ. (For interpretation of the references to color in this figure legend, the reader is referred to the web version of this article.)

was again primed for highly explosive activity (evolved, water-rich magmas).

The caldera collapse of Nisyros may have led to a restructuring of the upper-crustal mush system, and its growth towards the north. The restructuring resulted in the formation of a second eruptible magma chamber under the present-day island of Yali, which favored melt segregation and the formation of Yali-type crystal-poor, highly evolved melt pockets (Di Paola, 1974; Popa et al., 2019). This second magma reservoir erupted for the first time at 40 ± 5.2 ka, when a recharge event stimulated the magmatic system and triggered the Lower Yali explosion. The Upper Yali explosion occurred shortly soon after, at 35 ± 2.8 ka. After a larger repose period of ~12.3 ± 3.2 ky, an effusive eruption emplaced the rhyolitic Yali Obsidian at 22.7 ± 1.6 ka.

4.4. Time-dependency of effusive-explosive transitions

The eruptive style of the Nisyros-Yali rhyolitic magmas appears to be correlated with the length of the repose period that precedes each eruption (Fig. 5, B). It seems that shorter repose periods precede explosive events, while effusions follow after longer periods of volcanic rest. The sequence of eruption ages indicate that effusive events at Nisyros occurred after quiescence times of 45.4 ± 11.6 ky (Nikia) and 38.5 ± 3.1 ky (Post-Caldera Domes), which suggest recorded periods of volcanic rest of at least 33–35 ky. On the other hand, as the ages of the Lower and Upper Pumice indicate, the explosions at Nisyros occurred after an average repose period of 5–10 ky. Uncertainty considered, the recorded time window of explosivity at Nisyros could be extended to repose periods up to 18 ky. Similarly, the Upper Yali Pumice was erupted after a repose period of ~5 ky, which can be extended to ~11 ky considering the uncertainty of the ages. On the other hand, the effusive Yali Obsidian event took place after a longer quiescence of 12.3 ± 3.2 ky, allowing us to refine the 11–18 ky time window of potential explosivity to < 12 ky. Overall, it seems that the effusive-explosive transition at both Nisyros and Yali follows mainly a time-dependent scenario.

This observation is in agreement with our model on the effusive-explosive transitions at Nisyros-Yali (Popa et al., 2019). At both volcanoes, rhyolitic effusive eruptions were generated by magmas stored under water-supersaturated conditions, containing exsolved volatiles while still in the magma chamber. In contrast, rhyolitic explosive events were generated by water-undersaturated magmas. According to our model, water exsolution at storage pressure favors effusivity by increasing the bulk compressibility of the magma chamber and allowing higher volumes of hot recharge material to be accommodated pre-eruptively (Degruyter et al., 2017; Popa et al., 2019). This induces positive feedbacks between reheating, the drop in melt viscosity and the development of early gas permeability in the conduit, reducing the explosive potential of the magma.

In a simplified framework, the transition from a water-undersaturated to a water-supersaturated state is a continuum that depends dominantly on how long the system has to accumulate (dominantly incompatible) volatiles. Longer volcanic repose periods, similar to those preceding effusive events, allow more time for volatile build-up. This increases the likelihood of magmas becoming significantly water-supersaturated, when compared to the shorter repose periods that precede explosive events.

The time required to reach a water-supersaturated state is impacted by other factors, as well. An example is the starting condition of the differentiation process. This depends on the amount of water retained in the magma chamber after the outgassing event caused by the preceding eruption (i.e. initial water content). Equally, it depends on the degree of magma hybridization following the post-eruptive rejuvenation event of the upper-crustal silicic system. This impacts the composition of the melt (including its volatile concentration) and the temperature of the magma. There are also processes that can delay or accelerate the transition to a water-supersaturated state, after the differentiation process ensued. For example, subsequent smaller recharge events can interact with the upper-crustal magma chamber without triggering an eruption, given that sufficient overpressure is not induced (Degruyter et al., 2016). This can lead to volatile dilution (Cassidy et al., 2016), which delays the water-supersaturation of the magma. In contrast, CO_2 sparging caused by an underlying mafic magma can accelerate the water-saturation process (Newman and Lowenstern, 2002; Caricchi et al., 2018). Even in this complex context, the repose periods preceding the eruptions seem to offer an indication on the approximate timescales required for the Nisyros-Yali system to reach a water-supersaturated state. We can refer to this timescale as the explosive-effusive time-threshold.

The time-threshold for explosive to effusive transitions at Nisyros-Yali appears to be, on average, close to ~10–12 ky, with repose periods shorter than this value favoring explosivity. It is determined by comparing the repose periods preceding explosive events, which are observed with highest probability between 5 and 10 ky, to those preceding effusive events, which are between 12 and 45 ky at highest probability. However, considering the uncertainties associated with the age

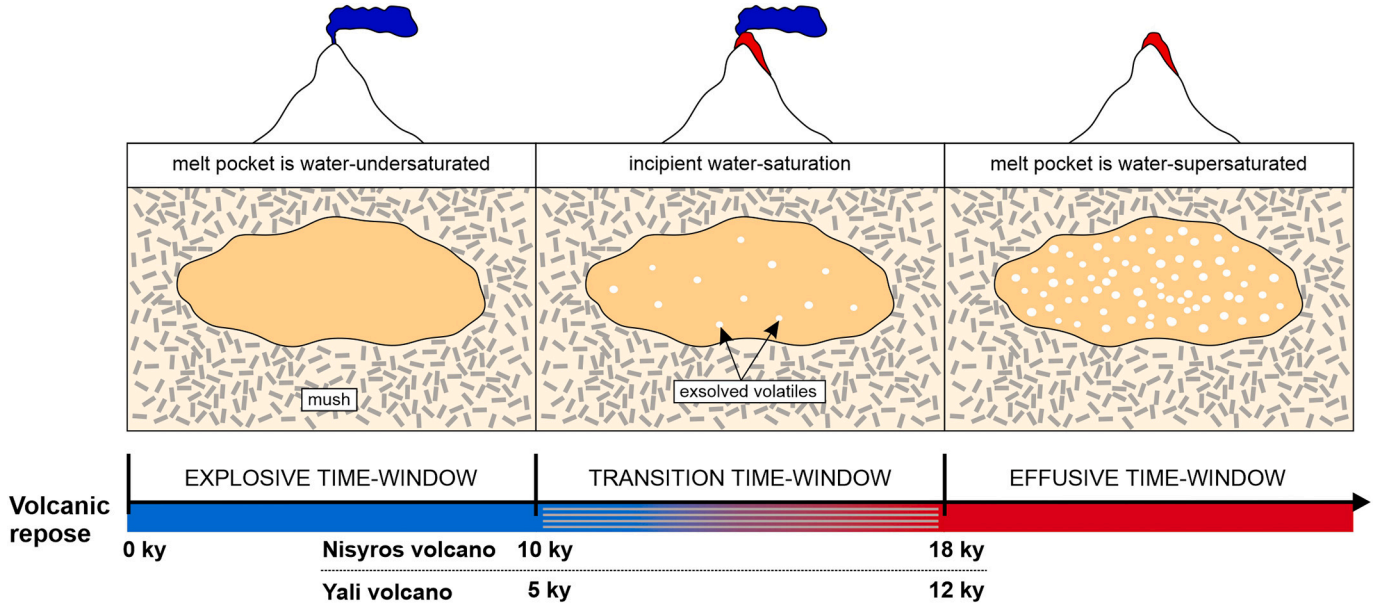

Fig. 6. Interpretative overview of the connection between eruptive styles at Nisyros and Yali volcanoes, and the volcanic repose periods preceding them. Longer periods of volcanic quiescence allow the eruptible melt pockets to differentiate to higher levels, attaining volatile-supersaturation and building higher volumes of exsolved volatiles. As briefly explained in the text, and detailed in Degruyter et al. (2017) and Popa et al. (2019), increasingly higher volumes of exsolved volatiles developed during magmatic storage increase the compressibility of the magma reservoir, and change its behavior during magmatic recharge. This influences the ensuing eruptive style. In the transition time window, both styles of eruption are likely to occur.

estimates and the likely decoupling between the Nisyros and Yali magma chambers, we consider it safer to assume that the explosive-effusive time-threshold for Nisyros is ~18 ky, and for Yali ~12 ky (Fig. 6). Considering that 19.9 ± 1.5 ky and 22.7 ± 1.6 ky have passed since the latest eruptions at Nisyros and Yali, respectively, both magma chambers could be currently in the effusive time window. This means that both magma chambers should be water-supersaturated at present. According to our model (Degruyter et al., 2017; Popa et al., 2019) it is currently more difficult to trigger eruptions and, in case of eruption triggering, effusive events are favored. The presence of exsolved volatiles in the magma reservoir could explain how the magma recharge event that generated the 1996–1997 earthquake crisis on Nisyros (Papadopoulos et al., 1998; Lagios et al., 2005) did not lead to an eruption: the recharge material was accommodated in the magma reservoir, and the overpressure was cushioned by the compressibility effect of the exsolved volatiles (Degruyter et al., 2017).

The recent work of Koutrouli et al. (2018) indicates the possibility that Yali could have generated minor explosions since the Obsidian event. The interpretation is based on two ash layers found in the vicinity of the island, but also on Yali. These are dated at ~10 ka and ~8 ka, respectively (Koutrouli et al., 2018). If the two layers are indeed sourced from Yali eruptions, their timing is in conformity with the time-threshold suggested: repose periods less than ~12 ky for Yali explosive activity. However, this raises the question of whether two minor events can have enough impact on the magma reservoir to reset the differentiation and water-supersaturation process significantly. If the two tephra layers are confirmed to be generated by Yali, then it might be possible for the magma chamber of this volcano to be in an explosive time window. However, Nisyros remains in a state that should favor effusivity.

5. Conclusions

The rhyolitic activity at Nisyros started with the Avlaki lava flow at 118.7 ± 10 ka. This occurred after nearly 40 ± 10 ky of volcanic activity involving basic and intermediate magmas, which likely represents the time required for the silicic upper-crustal mush to develop. The eruption of Avlaki was followed by the Nikia lava flow at 73.3 ± 5.8 ka, and by the two major caldera-forming eruptions: the Lower Pumice event at 63.1 ± 4.7 ka and the Upper Pumice event at 58.4 ± 2.7 ka. The youngest eruption on Nisyros emplaced the rhyodacitic Post-Caldera Domes at 19.9 ± 1.5 ka.

The rhyolitic activity at Yali started after the caldera collapse of Nisyros. The caldera collapse event likely caused the silicic upper-crustal mush to restructure, and has facilitated the formation of a crystal-poor melt pocket towards the north. The explosive eruptions of Yali occurred at 40 ± 5.2 ka and 35 ± 2.8 ka. The youngest eruption on Yali emplaced the rhyolitic Obsidian flow at 22.7 ± 1.6 ka.

Currently, the upper-crustal silicic mush contains at least two eruptible magma chambers, one below Nisyros and one under Yali. This points to a space-dependency of effusive-explosive transitions, as each magma chamber can evolve and erupt independently of the other. However, both magma chambers individually record time-dependency between eruptive styles. Repose periods longer than 18 ky for Nisyros and longer than 12 ky for Yali favor effusive events. This allows more time for volatile build-up, which increases the likelihood of the system becoming significantly water-supersaturated. Shorter repose periods favor explosive activity, which leads to an interesting possibility to forecast the style of the next eruption. Based on the length of the current volcanic quiescence period, the magma chambers of Nisyros and Yali have passed the explosive-effusive time-threshold. Hence, we forecast that both volcanoes are likely to behave effusively the next time they erupt. However, it is important to accurately determine whether the young (~10–8 ka) minor tephra layers found on Yali have been indeed generated by this volcano. If this is the case, it might imply that the explosive time window prevails at Yali.

Declaration of competing interest

The authors declare that they have no known competing financial interests or personal relationships that could have appeared to influence the work reported in this paper.

Acknowledgements

The authors thank Prof. Cyril Chelle-Michou and Dr. Marie Edmonds for constructive feedback on the manuscript, Dr. Jörn-Frederik Wotzlaw and Dr. Jakub Sliwinski for assistance in separating zircon crystals, Prof. Frank C. Ramos for the MC-ICPMS analyses of bulk-rock isotopic ratios, and Sergiu-Florin Popa for assisting in coding the Iterative-MSWD. We would like to thank Prof. Balz Kamber, Dr. Emma Tomlinson and an anonymous reviewer for their constructive suggestions, which helped us improve this manuscript considerably. This work was supported by the Swiss National Science Foundation grant No. 200021_178928 to O.B.

Appendix A. Supplementary data

Supplementary data to this article can be found online at https://doi.org/10.1016/j.chemgeo.2020.119830.

References

Aksu, A.E., Jenner, G., Hiscot, R.N., Isler, E.B., 2008. Occurrence, stratigraphy and geochemistry of Late Quaternary tephra layers in the Aegean Sea and the Marmara Sea. Mar. Geol. 252, 174–192.

Allen, S.R., McPhie, J., 2000. Water-settling and resedimentation of submarine rhyolitic pumice at Yali, eastern Aegean, Greece. J. Volcanol. Geotherm. Res. 95, 285–307.

Bachmann, O., Schoene, B., Schnyder, C., Spikings, R., 2010. The $^{40}Ar/^{39}Ar$ and U/Pb dating of young rhyolites in the Kos-Nisyros volcanic complex, Eastern Aegean Arc, Greece: age discordance due to excess ^{40}Ar in biotite. Geochem. Geophys. Geosyst. 11. https://doi.org/10.1029/2010GC003073.

Bachmann, O., Deering, C., Ruprecht, J.S., Huber, C., Skopelitis, A., Schnyder, C., 2012. Evolution of silicic magmas in the Kos-Nisyros volcanic center, Greece: a petrological cycle associated with caldera collapse. Contrib. Mineral. Petrol. 163, 151–166.

Bachmann, O., Allen, S.R., Bouvet de Maisonneuve, C., 2019. The Kos-Nisyros-Yali Volcanic Field. Elements 15, 191–196.

Barberi, F., Navarro, J.M., Rosi, M., Santacroce, R., Sbrana, A., 1988. Explosive interaction of magma with groundwater: insights from xenoliths and geothermal drillings. Rend. Soc. Ital. Mineral. Petrol. 43, 901–926.

Black, L.P., Kamo, S.L., Allen, C.M., Davis, D.W., Aleinikoff, J.N., Valley, J.W., Mundil, R., Campbell, I.H., Korsch, R.J., Williams, I.S., Foudoulis, C., 2004. Improved $^{206}Pb/^{238}U$ microprobe geochronology by the monitoring of a trace-element related matrix effect; SHRIMP, ID-TIMS, ELA-ICP-MS and oxygen isotope documentation for a series of zircon standards. Chem. Geol. 205, 115–140.

Caricchi, L., Sheldrake, T.E., Blundy, J., 2018. Modulation of magmatic processes by CO_2 flushing. Earth Planet. Sci. Lett. 491, 160–171.

Cassidy, M., Castro, J.M., Helo, C., Troll, V.R., Deegan, F.M., Muir, D., Neave, D.A., Mueller, S.P., 2016. Volatile dilution during magma injections and implications for volcano explosivity. Geology 44, 1027–1030.

Cassidy, M., Manga, M., Cashman, K., Bachmann, O., 2018. Controls on explosive-effusive volcanic eruption styles. Nat. Commun. 9, 2839. https://doi.org/10.1038/s41467-018-05293-3.

Chen, Y., Smith, P.E., Evensen, N.M., York, D., Lajoie, K.R., 1996. The edge of time: dating young volcanic ash layers with the $^{40}Ar/^{39}Ar$ laser probe. Science 274, 1176–1178.

Danišík, M., Schmitt, A., Stockli, D., Lovera, O., Dunkl, I., Evans, N., 2016. Application of combined U-Th-disequilibrium/U-Pb and (U-Th)/He zircon dating to tephrochronology. Quat. Geochronol. 40, 23–32.

Degruyter, W., Huber, C., Bachmann, O., Cooper, K.M., Kent, A.J.R., 2016. Magma reservoir response to transient recharge events: the case of Santorini volcano (Greece). Geology 44, 23–26.

Degruyter, W., Huber, C., Bachmann, O., Cooper, K.M., Kent, A.J.R., 2017. Influence of exsolved volatiles on reheating silicic magmas by recharge and consequences for eruptive style at Volcan Quizapu (Chile). Geochem. Geophys. Geosyst. https://doi.org/10.1002/2017GC007219.

Di Paola, G.M., 1974. Volcanology and petrology of Nisyros (Dodecanese, Greece). Bull. Volcanol. 38, 944–987.

Dietrich, J.V., 2018. Geology of Nisyros Volcano. In: Dietrich, J.V., Lagios, E. (Eds.), Nisyros Volcano. Springer, Active Vocanoes of the World series, pp. 57–102.

Federman, A.N., Carey, S.N., 1980. Electron microprobe correlation of tephra layers from Eastern Mediterranean abyssal sediments and the Island of Santorini. Quat. Res. 13, 160–171.

Gençalioğlu-Kuşcu, G., Uslular, G., Danišik, M., Koppers, A., Miggins, D.P., Friedrichs, B., Schmitt, A.K., 2020. U–Th disequilibrium, (U–Th)/He and $^{40}Ar/^{39}Ar$ geochronology of distal Nisyros Kyra tephra deposits on Datça peninsula (SW Anatolia). Quat. Geochronol. 55, 101033.

Guillong, M., Meier, D., Allan, M., Heinrich, C., Yardley, B., 2008. SILLS: a MATLAB-based program for the reduction of laser ablation ICP-MS data of homogeneous materials and inclusions. In: Sylvester, P. (Ed.), Laser Ablation ICP–MS in the Earth Sciences: Current Practices and Outstanding Issues. Mineralogical Association of Canada, Short Course Series. Vancouver, pp. 328–333.

Guillong, M., von Quadt, A., Sakata, S., Peytcheva, I., Bachmann, O., 2014. LA-ICP-MS Pb–U dating of young zircons from the Kos–Nisyros volcanic centre, SE Aegean arc. J. Anal. At. Spectrom. 29, 963–970.

Guillong, M., Sliwinski, J.Y., Schmitt, A., Forni, F., Bachmann, O., 2016. U-Th zircon dating by laser ablation single collector inductively coupled plasma-mass spectrometry (LA-ICP-MS). Geostand. Geoanal. Res. 40, 377–387.

Harangi, S., Lukács, R., Schmitt, A.K., Dunkl, I., Molnár, K., Kiss, B., Seghedi, I., Novothny, Á., Molnár, M., 2015. Constraints on the timing of Quaternary volcanism and duration of magma residence at Ciomadul volcano, east–central Europe, from combined U–Th/He and U–Th zircon geochronology. J. Volcanol. Geotherm. Res. 301, 66–80.

Hardiman, J.C., 1999. Deep sea tephra from Nisyros Island, eastern Aegean Sea, Greece. Geol. Soc. Spec. Publ. 161, 69–88.

Hollocher, K.T., Ruiz, J., 2007. Major and trace element determinations on NIST glass standard reference materials 611, 612, 614 and 1834 by inductively coupled plasma-mass spectrometry. Geostand. Geoanal. Res. 19, 27–34.

Karkanas, P., White, D., Lane, C.S., Stringer, C., Davies, W., Cullen, V.L., Smith, V.C., Ntinou, M., Tsartsidou, G., Kyparissi-Apostolika, N., 2015. Tephra correlations and climatic events between the MIS6/5 transition and the beginning of MIS3 in Theopetra Cave, central Greece. Quat. Sci. Rev. 118, 170–181.

Keller, C.B., Schoene, B., Samperton, K.M., 2018. A stochastic sampling approach to zircon eruption age interpretation. Geochemical Perspectives 8, 31–35.

Koutrouli, A., Anastasakis, G., Kontakiotis, G., Ballengee, S., Kuehn, S., Pe-Piper, G., Piper, D.J.W., 2018. The early to mid-Holocene marine tephrostratigraphic record in the Nisyros-Yali-Kos volcanic center, SE Aegean Sea. J. Volcanol. Geotherm. Res. 366, 96–111.

Lagios, E., Sakkas, V., Parcharidis, Is, Dietrich, V., 2005. Ground deformation of Nisyros Volcano (Greece) for the period 1995–2002: results from DInSAR and DGPS observations. Bull. Volcanol. 68, 201–214.

Laumonier, M., Karakas, O., Bachmann, O., Gaillard, F., Lukács, R., Seghedi, I., Menand, T., Harangi, S., 2019. Evidence for a persistent magma reservoir with large melt content beneath an apparently extinct volcano. Earth Planet. Sci. Lett. 521, 79–90.

Limburg, E.M., Varekamp, J.C., 1991. Young pumice deposits on Nisyros, Greece. Bull. Volcanol. 54, 68–77.

Lowenstern, J.B., Persing, H.M., Wooden, J.L., Lanphere, M., Donnelly-Nolan, J., Grove, T.L., 2000. U-Th dating of single zircons from young granitoid xenoliths: new tools for understanding volcanic processes. Earth Planet. Sci. Lett. 183, 291–302.

Margari, V., Pyle, D.M., Bryant, C., Gibbard, P.L., 2007. Mediterranean tephra stratigraphy revisited: results from a long terrestrial sequence on Lesvos Island, Greece. J. Volcanol. Geotherm. Res. 163, 34–54.

Newman, S., Lowenstern, J.B., 2002. VolatileCalc: a silicate melt-H2O-CO2 solution model written in Visual Basic for excel. Comput. Geosci. 28, 597–604.

Papadopoulos, G.A., Sachpazi, M., Panopoulou, G., Stavrakakis, G., 1998. The volcano-seismic crisis of 1996–97 in Nisyros, SE Aegean Sea, Greece. Terra Nova 10, 151–154.

Pe-Piper, G., Piper, D.J.W., 2005. The South Aegean active volcanic arc: relationships between magmatism and tectonics. Developments in Volcanology 7, 113–133.

Popa, R.-G., Bachmann, O., Ellis, B.S., Degruyter, W., Tollan, P., Kyriakopoulos, K., 2019. A connection between magma chamber processes and eruptive styles revealed at Nisyros-Yali volcano (Greece). J. Volcanol. Geotherm. Res. https://doi.org/10.1016/j.jvolgeores.2019.106666.

Popa, R.-G., Dietrich, V.J., Bachmann, O., 2020. Effusive-explosive transitions of water-undersaturated magmas. The case study of Methana Volcano, South Aegean Arc. J. Volcanol. Geotherm. Res. 399, 106884.

Pyle, D.M., Margari, V., 2009. Reply: Correlation of a widespread Pleistocene tephra marker from the Nisyros-Yali volcanic complex, Greece. J. Volcanol. Geotherm. Res. 181, 251–254.

Ramos, F.C., Heizler, M.T., Buettner, J.E., Gill, J.B., Wei, H.Q., Dimond, C.A., Scott, S.R., 2016. U-series and 40Ar/39Ar ages of Holocen volcanic rocks at Changbaishan volcano, China. Geology 44, 511–514.

Rehren, T., 1988. Geochemie und Petrologie von Nisyros (Östliche Ägäis). University of Freiburg, pp. 167.

Rocholl, A., 2007. Major and trace element composition and homogeneity of microbeam reference material: basalt glass USGS BCR-2G. Geostand. Geoanal. Res. 22, 33–45.

Ruprecht, P., Bachmann, O., 2010. Pre-eruptive reheating during magma mixing at Quizapu volcano and the implications for the explosiveness of silicic arc volcanoes. Geology 38, 919–922.

Satow, C., Tomlinson, E.L., Grant, K.M., Albert, P.G., Smith, V.C., Manning, C.J., Ottolini, L., Wulf, S., Rohling, E.J., Lowe, J.J., Blockey, S.P.E., Menzies, M.A., 2015. A new contribution to the late Quaternary tephrostratigraphy of the Mediterranean: Aegean Sea core LC21. Quat. Sci. Rev. 117, 96–112.

Scaillet, S., Vita-Scaillet, G., Rotolo, S.G., 2013. Millennial-scale phase relationships between ice-core and Mediterranean marine records: insights from high-precision $^{40}Ar/^{39}Ar$ dating of the Green Tuff of Pantelleria, Sicily Strait. Quat. Sci. Rev. 78, 141–154.

Schmitt, A.K., 2011. Uranium series accessory crystal dating of magmatic processes. Annu. Rev. Earth Planet. Sci. 39, 321–349.

Schmitz, M.D., Bowring, S.A., 2001. U-Pb zircon and titanite systematics of the Fish Canyon Tuff: an assessment of high-precision U-Pb geochronology and its application to young volcanic rocks. Geochim. Cosmochim. Acta 65, 2571–2587.

Simon, J.I., Renne, P.R., Mundil, R., 2008. Implications of pre-eruptive magmatic histories of zircons for U-Pb geochronology of silicic extrusions. Earth Planet. Sci. Lett. 266, 182–194.

Sláma, J., Košler, J., Condon, D.J., Crowley, J.L., Gerdes, A., Hanchar, J.M., Horstwood, M.S.A., Morris, G.A., Nasdala, L., Norberg, N., Schaltegger, U., Schoene, B., Tubrett, M.N., Whitehouse, M.J., 2008. Plešovice zircon – new natural reference material for U-Pb and Hf isotopic microanalysis. Chem. Geol. 249, 1–35.

Szymanowski, D., Wotzlaw, J.-F., Ellis, B.S., Bachmann, O., Guillong, M., von Quadt, A., 2017. Protracted near-solidus storage and pre-eruptive rejuvenation of large magma

reservoirs. Nat. Geosci. 10, 777–782.
Szymanowski, D., Ellis, B.S., Wotzlaw, J.-F., Bachmann, O., 2019. Maturation and rejuvenation of a silicic magma reservoir: high-resolution chronology of the Kneeling Nun Tuff. Earth Planet. Sci. Lett. 510, 103–115.
Tomlinson, E.L., Kinvig, H.S., Smith, V.C., Blundy, J.D., Gottsmann, J., Müller, W., Menzies, M.A., 2012. The Upper and Lower Nisyros Pumices: revisions to the Mediterranean tephrostratigraphic record based on micron-beam glass geochemistry. J. Volcanol. Geotherm. Res. 243-244, 69–80.
Vermeesch, P., 2018. IsoplotR: a free and open toolbox for geochronology. Geosci. Front. 9, 1479–1493.
Vinci, A., 1985. Distribution and chemical composition of tephra layers from eastern Mediterranean abyssal sediments. Mar. Geol. 64, 143–155.
Wagner, G.J., Storzer, D., Keller, J., 1976. Spalltspurendatierungen quartarer Gesteinsglaser aus dem Mittelmeerraum. Neues Jb. Mineral. Abh. 2, 84–94.
Wiedenbeck, M., Allé, P., Corfu, F., Griffin, W.L., Meier, M., Oberli, F., von Quadt, A., Roddick, J.C., Speigel, W., 1995. Three natural zircon standards for U-Th-Pb, Lu-Hf, trace-element and REE analyses. Geostand. Newslett. 19, 1–23.
Wotzlaw, J.-F., Schaltegger, U., Frick, D.A., Dungan, M.A., Gerdes, A., Günther, D., 2013. Tracking the evolution of large-volume silicic magma reservoirs from assembly to supereruption. Geology 41, 867–870.